

# Effective capacity analysis of full-duplex-cooperative non-orthogonal multiple access systems

Huu Q. Tran<sup>1</sup>, Samarendra Nath Sur<sup>2</sup>

<sup>1</sup>Faculty of Electronics Technology, Industrial University of Ho Chi Minh City, Ho Chi Minh City, Vietnam

<sup>2</sup>Department of Electronics and Communication Engineering, Sikkim Manipal Institute of Technology, Sikkim Manipal University, Sikkim, India

## Article Info

### Article history:

Received Jul 12, 2023

Revised May 8, 2024

Accepted May 26, 2024

### Keywords:

Effective capacity

Full-duplex

Multi-reconfigurable intelligent surfaces

Non-orthogonal multiple access

Outage probability

## ABSTRACT

This study explores a dual-user full-duplex cooperative non-orthogonal multiple access (FD-CNOMA) network, presenting closed-form expressions for the outage probability (OP) and effective capacity (EC) of both users. The analytical results indicate that an increased signal-to-noise ratio (SNR) corresponds to a reduced OP and heightened EC, signifying enhanced communication quality. We analyze the OP and EC under two cases:  $R_1=2R_2$  and  $R_1=R_2$ . Our analytical expressions reveal that both  $\theta$  and  $\rho$  significantly impact the effective capacities. To validate these analytical findings, Monte Carlo simulations are performed, demonstrating alignment between theoretical insights and practical outcomes. The results underscore the critical role of SNR in influencing network performance, providing valuable insights into optimizing communication quality in FD-CNOMA systems.

*This is an open access article under the [CC BY-SA](#) license.*



## Corresponding Author:

Huu Q. Tran

Faculty of Electronics Technology, Industrial University of Ho Chi Minh City

Ho Chi Minh City, Vietnam

Email: tranquyhuu@iuh.edu.vn

## 1. INTRODUCTION

Non-orthogonal multiple access (NOMA) has emerged as a promising technology for enhancing the spectral efficiency and capacity of future wireless communication systems. By allowing multiple users to share the same time-frequency resources, NOMA enables the simultaneous transmission and reception of multiple signals within a single resource block. Recent research has highlighted the potential applicability of NOMA in a variety of sixth-generation (6G) transmission scenarios, particularly in the context of machine-to-machine (M2M) connections and the internet of things (IoT) [1]–[6]. Moreover, there is evidence to suggest that the effectiveness of NOMA can be further enhanced when integrated with various other advanced mobile communication techniques. These techniques encompass shared interactions, multiple-input multiple-output (MIMO) technology [7], beamforming, space-time programming for IoT networks, and the utilization of full-duplex (FD) communication [8]. Recently, FD communication has gained significant attention as a means to further improve the capacity and efficiency of wireless networks. Unlike traditional half-duplex (HD) communication, where a node can either transmit or receive signals at a given time, FD communication enables simultaneous transmission and reception in the same frequency band [9], [10]. This self-interference cancellation technique has the potential to double the spectral efficiency and capacity of wireless systems. Furthermore, cooperative communication has been empirically shown to offer several advantages. It extends network coverage, enhances

connectivity reliability, and boosts system capacity by enabling users within a network to collaborate in relaying information [11], [12]. FD-cooperative NOMA has emerged as a new paradigm that combines the benefits of FD communication and NOMA to achieve even higher capacity gains. In FD-cooperative NOMA, multiple users are grouped together as clusters, and each cluster consists of a FD base station (BS) and several HD users. The FD BS acts as a relay for the users within the cluster, enabling simultaneous transmission and reception in both the uplink and downlink directions [13], [14]. Hussain [15], investigated a hybrid FD and HD user relaying system in the context of NOMA. It employs an advanced successive interference cancellation (ASIC) scheme as an alternative to the traditional successive interference cancellation (SIC) method. The proposed system aims to enhance efficiency compared to both conventional systems and ASIC-based FD NOMA systems with dedicated relaying nodes. The study of the fundamental limits of FD spectrum sharing in cognitive radio (CR) networks under a peak interference power constraint can be found in [16].

To analyze the performance of cooperative NOMA systems, it is crucial to evaluate their effective capacity (EC). EC is a metric that characterizes the maximum achievable rate at which information can be reliably transmitted over a communication channel, accounting for both the average and bursty nature of the traffic. By considering the delay and reliability requirements of different applications, EC provides a comprehensive measure of system performance [17], [18]. Huang *et al.* [19], explored the efficacy of EC in a NOMA network, considering residual hardware impairments and imperfections in serial interference cancellation. Li *et al.* [20], a system framework known as ambient backscatter communication-NOMA (AmBC-NOMA) was introduced by the authors. They also went on to derive precise expressions for the EC of both NOMA users and the backscatter device. Additionally, for a deeper understanding, the authors conducted an asymptotic analysis by utilizing high signal-to-noise ratio (SNR) slope and a high SNR power offset approach.

In this paper, we present a comprehensive analysis of the EC of FD-cooperative NOMA systems. We consider a realistic wireless channel model that captures the effects of fading, interference, and self-interference cancellation in FD communication. We derive analytical expressions for the EC under various system configurations and investigate the impact of key parameters such as the target rates, power allocation, and quality-of-service exponent ( $\theta$ ).

The remainder of this paper is organized as follows. Section 2 presents the system model and outlines the key assumptions and parameters considered in our analysis. Section 3 analyzes the outage performance at users. In section 4, we derive the analytical expressions for the eEC of FD-cooperative NOMA systems. Section 5 presents numerical results and discusses the insights gained from our analysis. Finally, section 6 concludes the paper and highlights directions for future research.

## 2. SYSTEM MODEL

Consider a FD cooperative NOMA system with a BS that aims to interact with two users, namely distant user 1 ( $U_1$ ) and close user 2 ( $U_2$ ), as depicted in Figure 1. In this system,  $U_1$  serves as the relay user, employing the decode-and-forward (DF) protocol to forward information to  $U_2$ .  $U_1$  is equipped with one broadcast and one receive antenna to support FD communication, while both the BS and  $U_2$  are single-antenna nodes. All wireless connections in the network are assumed to experience non-selective block Rayleigh fading, along with additive white Gaussian noise with a mean power of  $\sigma^2$ . The complex channel coefficients for the connections between the BS and  $U_1$ , as well as  $U_2$  and  $U_1$ , are denoted as  $g_1$  and  $g_2$ , respectively. The channel power gains, represented by  $|g_1|^2$  and  $|g_2|^2$ , are considered to be exponentially distributed random variables (RVs) with parameters  $\lambda_1$  and  $\lambda_2$ . It is assumed that when  $U_1$  operates in FD mode, it utilizes an imperfect self-interference cancellation mechanism. The loop self-interference (LI) is modeled as a Rayleigh fading channel with a coefficient of  $|g_{LI}|^2$  and an average power of  $\lambda_{LI}$ . In the  $n$ -th time slot, the BS transmits a superimposed message to  $U_1$ , given by:

$$s[n] = \sqrt{P_S a_1} s_1[n] + \sqrt{P_S a_2} s_2[n], \quad (1)$$

Where  $s_1$  and  $s_2$  represent the signals for  $U_1$  and  $U_2$ , respectively, satisfying  $\mathbb{E}\{|s_1|^2\} = \mathbb{E}\{|s_2|^2\} = 1$ , where  $\mathbb{E}[x]$  denotes the expectation operation.  $P_S$  denotes the transmitted power of the BS, while  $a_1$  and  $a_2$  are the power allocation coefficients for  $U_1$  and  $U_2$ , respectively, subject to  $a_1 < a_2$  and  $a_1 + a_2 = 1$ . Following the NOMA cooperation principle,  $U_1$  can decode the message of  $U_2$ , whether it is successfully decoded or not, and we consider  $s_2$  as the message at  $U_1$ . According to Yue *et al.* [21], during the  $n$ -th time slot,  $U_1$  simultaneously

receives the superimposed signal and the self-interference (SI) signal.  $U_1$ 's observations are provided by:

$$y_{U_1}[n] = g_1 s[n] + g_{LI} \sqrt{P_{U_1}} s_{LI}[n - \tau] + \omega_{U_1}[n], \quad (2)$$

Where  $s_{LI}[n - \tau]$  represents the loop interference signal and  $\tau$  denotes the processing delay at  $U_1$ , with an integer  $\tau \geq 1$ . Specifically, we assume that the time  $n$  satisfies the relationship  $n \geq \tau$ .  $P_{U_1}$  represents the normalized transmission power at  $U_1$ , and we assume  $P_{U_1} = P_S$ .  $\omega_{U_i} \sim \mathcal{CN}(0, \sigma^2)$ ,  $i \in \{1, 2\}$ , represents complex additive white Gaussian noise with a mean of 0 and a variance of  $\sigma^2$ . Assuming perfect SIC, the received signal-to-interference-plus-noise ratio (SINR) of  $U_1$  decoding  $U_2$ 's signal  $s_2[n]$  and  $U_1$  decoding its own signal  $s_1[n]$  are given by:

$$\begin{aligned} \gamma_{U_1, x_2} &= \frac{a_2 P_S |g_1|^2}{a_1 P_S |g_1|^2 + P_{U_1} |g_{LI}|^2 + \sigma^2} \\ &= \frac{a_2 \rho |g_1|^2}{a_1 \rho |g_1|^2 + \rho |g_{LI}|^2 + 1}, \end{aligned} \quad (3a)$$

$$\gamma_{U_1, x_1} = \frac{a_1 \rho |g_1|^2}{\rho |g_{LI}|^2 + 1}, \quad (3b)$$

Where  $\rho = \frac{P_S}{\sigma^2}$  represents the transmit SNR. Note that  $s_{LI}$  is assumed to be a normalized unity power signal, i.e.,  $\mathbb{E}\{|s_{LI}|^2\} = 1$ .

The received signal at  $U_2$  can be expressed as (4):

$$y_{U_2}[n] = g_2 \sqrt{P_{U_1}} s_2[n] + \omega_{U_2}[n] \quad (4)$$

The SNR at  $U_2$  when detecting  $s_2[n]$  can be expressed as (5):

$$\begin{aligned} \gamma_{U_2, x_2} &= \frac{P_{U_1} |g_2|^2}{\sigma^2} \\ &= \rho |g_2|^2. \end{aligned} \quad (5)$$

Additionally, the Rayleigh-distributed random variables  $|g_o|^2$ , where  $o \in \{1, 2, LI\}$ , have exponential distributions with probability density function  $f_{|g_o|^2} = \frac{1}{\lambda_o} e^{-\frac{x}{\lambda_o}}$  and cumulative distribution function  $F_{|g_o|^2} = 1 - e^{-\frac{x}{\lambda_o}}$  [22].

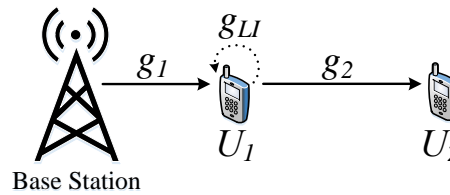


Figure 1. System model of the FD-NOMA communication system

### 3. OUTAGE PROBABILITY

Outage probability (OP) is an important statistic for evaluating performance, particularly when the desired rate of users is determined by their quality of service (QoS) requirements. It helps in understanding how often the system fails to meet the expected performance standards. In the following section, we will assess the outage performance of two users.

#### 3.1. OP at $U_1$

The complementing events of the outage at  $U_1$  can be explained using the NOMA protocol as follows: In NOMA,  $U_1$  has the capability to decode not only its own message ( $s_1$ ) but also the message intended for  $U_2$  ( $s_2$ ). OP at  $U_1$  can be expressed as follows, based on the previous description:

$$\mathcal{O}_{U_1} = 1 - \Pr(\gamma_{U_1, x_2} > \varepsilon_2, \gamma_{U_1, x_1} > \varepsilon_1), \quad (6)$$

where  $\varepsilon_1 = 2^{R_1} - 1$ , with  $R_1$  being the target rate at  $U_1$  to detect  $s_1$ , and  $\varepsilon_2 = 2^{R_2} - 1$ , with  $R_2$  being the target rate at  $U_1$  to detect  $s_2$ . The subsequent theorem presents a formula for computing OP at  $U_1$  in FD-NOMA. The closed-form expression for OP at  $U_1$  is as (7):

$$\begin{aligned} \mathcal{O}_{U_1} &= 1 - \Pr\left(|g_1|^2 > \phi_{\max}(\rho|g_{LI}|^2 + 1)\right) \\ &= 1 - \int_0^{\infty} f_{|g_{LI}|^2}(x) \left[1 - F_{|g_1|^2}(\phi_{\max}(\rho x + 1))\right] dx \\ &= 1 - \frac{\lambda_1}{\lambda_1 + \rho\phi_{\max}\lambda_{LI}} e^{-\frac{\phi_{\max}}{\lambda_1}}, \end{aligned} \quad (7)$$

where  $\phi_{\max} = \max(\phi_1, \phi_2)$ ,  $\phi_1 = \frac{\varepsilon_1}{a_1\rho}$ , and  $\phi_2 = \frac{\varepsilon_2}{\rho(a_2 - \varepsilon_2 a_1)}$ . Note that (7) is derived under the condition of  $a_2 > \varepsilon_2 a_1$ . Utilizing the analytical outcome from (7), when  $\rho$  approaches infinity ( $\rho \rightarrow \infty$ ), the asymptotic OP at  $U_1$  for FD-NOMA, using the approximation  $e^{-x} \approx 1 - x$ , is as (8):

$$\mathcal{O}_{U_1}^{\infty} = 1 - \frac{\lambda_1}{\lambda_1 + \rho\phi_{\max}\lambda_{LI}}. \quad (8)$$

### 3.2. OP at $U_2$

The occurrences of outage for  $U_2$  can be discussed as: The first scenario is when  $U_1$  is unable to correctly identify and decode  $s_2$ . In this case,  $U_2$  will experience an outage. The second scenario is when  $U_2$  is unable to detect its own message,  $s_2$ , even though  $U_1$  is successfully able to detect and decode it. Under these conditions,  $U_2$  will also experience an outage. Based on these scenarios, OP at  $U_2$  can be given as (9):

$$\mathcal{O}_{U_2} = 1 - \Pr(\gamma_{U_1, x_2} > \varepsilon_2, \gamma_{U_2, x_2} > \varepsilon_2). \quad (9)$$

The following theorem furnishes OP at  $U_2$  in FD NOMA.

$$\begin{aligned} \mathcal{O}_{U_2} &= 1 - \Pr\left(|g_1|^2 > \phi_2(\rho|g_{LI}|^2 + 1), |g_2|^2 > \frac{\varepsilon_2}{\rho}\right) \\ &= 1 - \int_0^{\infty} \int_{\frac{\varepsilon_2}{\rho}}^{\infty} f_{|g_{LI}|^2}(x) f_{|g_2|^2}(y) \left[1 - F_{|g_1|^2}(\phi_2(\rho x + 1))\right] dx dy \\ &= 1 - \frac{\lambda_1}{\lambda_1 + \rho\phi_2\lambda_{LI}} e^{-\frac{\phi_2}{\lambda_1} - \frac{\varepsilon_2}{\rho\lambda_2}}. \end{aligned} \quad (10)$$

Using the (10), the asymptotic OP at  $U_2$  in FD-NOMA is expressed as (11):

$$\mathcal{O}_{U_2}^{\infty} = 1 - \frac{\lambda_1}{\lambda_1 + \rho\phi_2\lambda_{LI}}. \quad (11)$$

## 4. EFFECTIVE CAPACITY ANALYSIS

EC takes into account system delay and is considered a more reasonable evaluation metric. EC is defined as the maximum constant arrival rate that a transmitter can achieve while satisfying QoS constraints [23]. Mathematically, it can be expressed as (12):

$$\begin{aligned} \mathcal{R}(\theta) &= -\frac{1}{\theta TB} \ln(\mathbb{E}\{e^{-\theta TB\gamma}\}) \\ &= -\frac{1}{\Theta} \log_2\left(\mathbb{E}\{(1 + \gamma)^{-\Theta}\}\right), \end{aligned} \quad (12)$$

where  $\Theta = TB\theta/\ln 2$ , with  $B$  being the bandwidth and  $T$  being the block length. The QoS exponent, denoted by  $\theta$ , is a positive value, and it is given by:

$$\theta = -\lim_{x \rightarrow \infty} \frac{\ln \Pr[Q > x]}{x}, \quad (13)$$

where  $Q$  is the equilibrium queue-length of the buffer at the transmitter.

#### 4.1. EC of the $U_1$

For  $U_1$ , assuming  $U_1$  successfully decodes  $s_2$ , the EC can be obtained as (14):

$$\mathcal{R}_{U_1} = -\frac{1}{\Theta} \log_2 \left( \mathbb{E} \left[ (1 + \gamma_{U_1, x_2})^{-\Theta} \right] \right), \quad (14)$$

Upon substituting (3b) into (14), we obtain EC,  $\mathcal{R}_{U_1}$  for  $U_1$  as (15):

$$\mathcal{R}_{U_1} = -\frac{1}{\Theta} \log_2 \left( \int_0^{\infty} (1+x)^{-\Theta} f_{\gamma_{U_1, x_2}}(x) dx \right). \quad (15)$$

From (7), we can calculate  $f_{\gamma_{U_1, x_2}}(x)$  as (16):

$$\begin{aligned} f_{\gamma_{U_1, x_2}}(x) &= \frac{\partial}{\partial x} F_{\gamma_{U_1, x_2}}(x) \\ &= \frac{e^{-\frac{x}{\lambda_1 a_1 \rho}} (x \lambda_{LI} + \lambda_1 a_1 + \lambda_1 a_1 \rho \lambda_{LI})}{\rho (\lambda_1 a_1 + x \lambda_{LI})^2} \end{aligned} \quad (16)$$

By substituting (16) into (15) and replacing the variable  $x = \lambda_1 a_1 \rho t$ , EC,  $\mathcal{R}_{U_1}$  is given by:

$$\mathcal{R}_{U_1} = -\frac{1}{\Theta} \log_2 \left( \lambda_1 a_1 \int_0^{\infty} \frac{e^{-t} (\lambda_1 a_1 \rho \lambda_{LI} t + \lambda_1 a_1 + \lambda_1 a_1 \rho \lambda_{LI})}{(\lambda_1 a_1 + \lambda_1 a_1 \rho \lambda_{LI} t)^2 (1 + \lambda_1 a_1 \rho t)^{\Theta}} dt \right). \quad (17)$$

The (17) can be further approximated using integral expressions through the Gauss-Laguerre quadrature method [24]. This method involves approximating the integral using a weighted sum of function evaluations at specific points known as the Gauss-Laguerre quadrature points. By utilizing this method, we can obtain a more efficient and accurate approximation in (17).

$$\mathcal{R}_{U_1} \approx -\frac{1}{\Theta} \log_2 \left( \lambda_1 a_1 \sum_{p=1}^P \mathcal{H}_p \frac{(\lambda_1 a_1 \rho \lambda_{LI} t_p + \lambda_1 a_1 + \lambda_1 a_1 \rho \lambda_{LI})}{(\lambda_1 a_1 + \lambda_1 a_1 \rho \lambda_{LI} t_p)^2 (1 + \lambda_1 a_1 \rho t_p)^{\Theta}} \right), \quad (18)$$

In the Gauss-Laguerre quadrature method,  $t_p$  represents the abscissas (quadrature points), while  $\mathcal{H}_p$  represents the weights associated with each point.  $t_p$  is the  $p$ -th zero of the Laguerre polynomial  $\mathcal{L}_p(t_p)$ , and  $\mathcal{H}_p$  can be formulated as  $\mathcal{H}_p = \frac{(P!)^2 t_p}{[\mathcal{L}_{P+1}(t_p)]^2}$ . Here, The parameter  $P$  plays a crucial role in balancing the trade-off between complexity and accuracy, allowing for a balance between the two. By selecting appropriate values for  $P$ , we can achieve the desired level of accuracy in the approximation.

#### 4.2. EC of the $U_2$

If we assume that  $U_1$  successfully decodes both  $s_2$  and  $s_1$ , then EC for  $U_2$  decoding  $s_2$  can be given by:

$$\begin{aligned} \mathcal{R}_{U_2} &= -\frac{1}{\Theta} \log_2 \left( \int_0^{\infty} (1+t)^{-\Theta} f_{\gamma_{U_2, x_2}}(t) dt \right) \\ &= -\frac{1}{\Theta} \log_2 \left( \frac{1}{\rho \lambda_2} \int_0^{\infty} (1+t)^{-\Theta} e^{-\frac{t}{\rho \lambda_2}} dt \right). \end{aligned} \quad (19)$$

With [25] (3.382.3) and [25] (9.220.2), the expression in (19) can be evaluated as (20):

$$\begin{aligned} \mathcal{R}_{U_2} &= -\frac{1}{\Theta} \log_2 \left( \frac{1}{(\rho \lambda_2)^{\frac{\Theta}{2}}} e^{\frac{1}{2\rho \lambda_2}} W_{-\frac{\Theta}{2}, \frac{(1-\Theta)}{2}} \left( \frac{1}{\rho \lambda_2} \right) \right) \\ &= -\frac{1}{\Theta} \log_2 \left( \frac{1}{\rho \lambda_2} U \left( 1, 2 - \Theta; \frac{1}{\rho \lambda_2} \right) \right), \end{aligned} \quad (20)$$

where  $W_{\lambda, \mu}(z)$  is the whittaker function defined as  $W_{\lambda, \mu}(z) = e^{-\frac{z}{2}} z^{\mu + \frac{1}{2}} U \left( \mu - \lambda + \frac{1}{2}, 1 + 2\mu; z \right)$  and  $U(\mu, k; z)$  is the confluent hypergeometric function, defined as  $U(\mu, k; z) = \frac{1}{\Gamma(\mu)} \int_0^{\infty} e^{-zt} t^{\mu-1} (1+t)^{k-\mu-1} dt$ , where  $\mu > 0$ .

## 5. RESULT AND DISCUSSION

In this section, we will evaluate the performance of the derived theoretical expression and validate it through numerical results. In the following figures, we denote 'Ana.' and 'Sim.' to represent analytical computation and Monte Carlo calculation-based simulations, respectively. To provide specific values for the parameters, we make the following assumptions:

- The distance between BS and  $U_1$  is normalized, with  $\lambda_1 = d^{-\alpha}$ , where  $d$  is set to 0.3 and  $\alpha$  is the path loss exponent, which is set to  $\alpha = 2$ .
- The distance between BS and  $U_2$  is  $\lambda_2 = (1 - d)^{-\alpha}$ .
- The power allocation coefficients for  $U_1$  and  $U_2$  in NOMA are  $a_1 = 0.2$  and  $a_2 = 0.8$ , respectively.
- The target rates for  $U_1$  and  $U_2$  are  $R_1 = 2$  and  $R_2 = 0.5$  bits per channel use (BPCU), respectively.
- For the Gauss-Laguerre quadrature, we select the parameter  $P = 100$  to achieve a close approximation [26].
- The value of LI is assumed to be  $\lambda_{LI} = 0.01$ .

Additionally, one of the technological contributions of our code is that we employ symbolic calculations in MATLAB to obtain highly accurate results. This ensures precise evaluation of the derived expressions. Figure 2 illustrates the outage performance with respect to  $R_1$  and  $R_2$ . The analytical findings are depicted in Figure 2, utilizing (7) and (10) from section 3. The markers in the figure correspond to the results of the Monte Carlo simulations (6) and (9). It is demonstrated that there exist error floors in FD-Cooperative NOMA, confirming the conclusions drawn in (8) and (11). However, in order to ensure reliable communication, it is important to choose a conservative target rate and ensure a sufficiently high SNR. Setting higher target rates may appear to constrain the outage performance. It is worth noting that NOMA networks encompass different power allocation factors, resulting in performance variations between distant NOMA users.

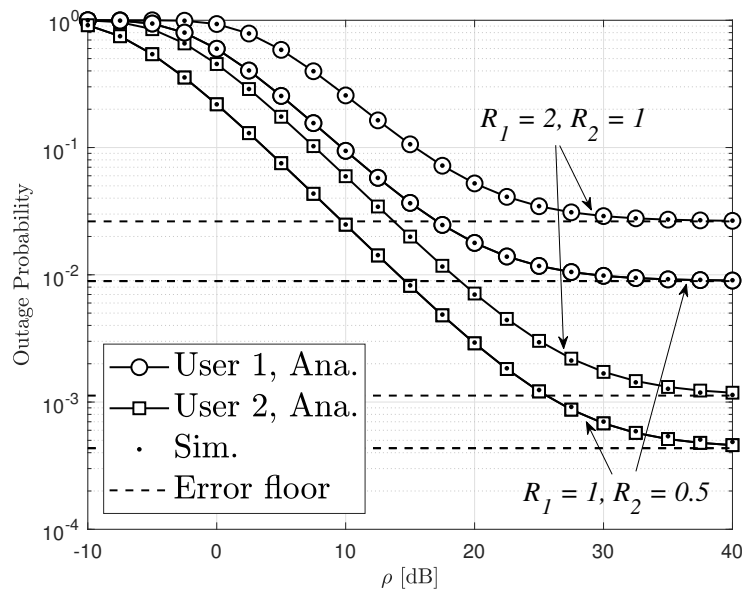


Figure 2. OP at  $U_1$  and  $U_2$  versus  $\rho$

Figure 3 represents a simulation of OP versus power allocation at  $U_2$ , assuming a certain level of system defects that can be considered inconsequential. From the graph, we can observe that as the power level for  $U_2$  increases, the performance of  $U_2$  improves, while the performance of  $U_1$  deteriorates. This is due to the power allocation requirement in NOMA, which states that  $a_1 + a_2 = 1$ . When the power allocation for both users becomes equal, at  $a_1 = a_2 = 0.5$ , the performance of both users becomes similar, and the curves converge at that point. Another important factor to consider is the impact of the transmitting SNR. As the transmitting SNR increases, the quality of signal transmission improves, leading to a lower OP at the users. This is why we can observe a significant gap between the curves on the graph. As the transmit SNR grows, the likelihood of outage decreases, resulting in improved performance for the user.

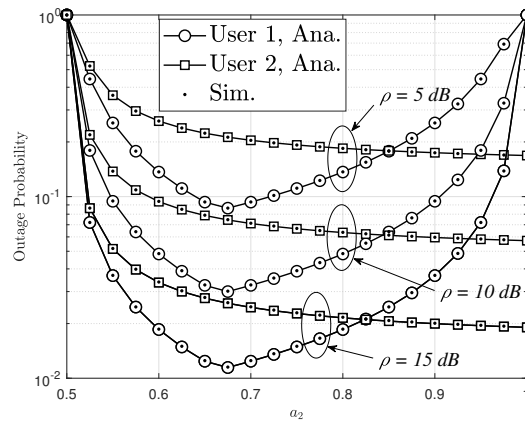


Figure 3. OP at  $U_1$  and  $U_2$  versus  $a_2$  with  $R_1 = R_2 = 1$

Figure 4 illustrates OP at both user  $U_1$  and user  $U_2$  as the goal rates  $R_1 = R_2$ , power allocation coefficients  $a_1 = 0.05$ ,  $a_2 = 0.95$ , and  $\rho$  (in dB) vary. This figure provides insight into how different values of  $R_1 = R_2$  impact the outage performance. By analyzing the data, we can understand the relationship between the goal rates and the observed outage probabilities.

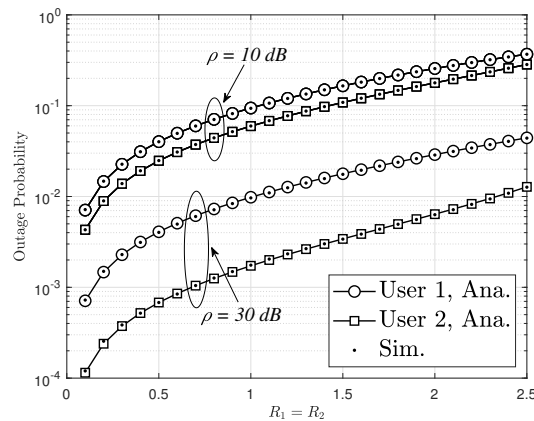


Figure 4. OP of  $U_1$  and  $U_2$  versus  $R_1$  and  $R_2$

It can be observed that the best outage performance (lowest OP) for both  $U_1$  and  $U_2$  is achieved when  $R_1 = R_2 = 0.3$  bit/s/Hz. Additionally, as the values of  $R_1 = R_2$  increase significantly, OP at  $U_1$  reaches a threshold or "ceiling" beyond which it does not decrease further. This suggests that higher levels of  $R_1 = R_2$  can significantly impact OP at  $U_1$ .

Figure 5 illustrates the impact of the QoS exponent  $\theta$  on EC, considering SNR values of 10 dB and 20 dB. EC curves for the two users are plotted based on (18) and (20). We varied  $\theta$  from 0 to 1, where a larger  $\theta$  indicates stricter delay requirements and consequently lower EC. As expected, we observe that as  $\theta$  increases, EC of both  $U_1$  and  $U_2$  decrease. This is because a larger  $\theta$  imposes more stringent delay constraints, limiting the maximum constant arrival rate that can be achieved. Furthermore, we can see that EC of  $U_1$  and  $U_2$  exhibit different levels of reduction when  $\theta$  is small. This is due to  $U_1$  having a higher SINR, resulting in a more pronounced decrease in its EC compared to  $U_2$ . Moreover, as  $\theta$  approaches 1, the change in EC becomes more gradual. This indicates that when the delay requirements are already stringent, further increasing  $\theta$  has a diminishing effect on EC. Additionally, we observe that an increase in SNR clearly enhances EC. This is consistent with the findings in Figure 2, where higher SNR values lead to improved performance and lower OPs.

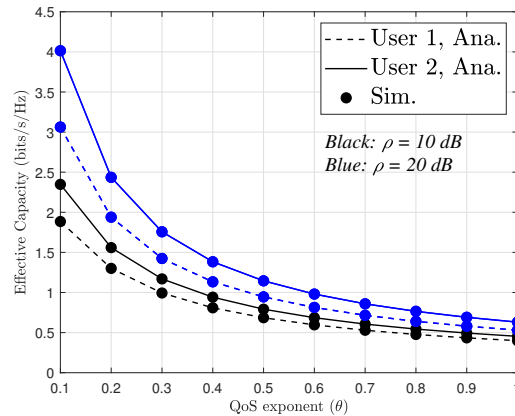


Figure 5. Effects of the QoS exponent  $\theta$  and different  $\rho$  on ECs

## 6. CONCLUSION

In this paper, we have studied OP and EC of NOMA schemes for two users. We have derived numerical results for NOMA protocols in two cases:  $R_1=2R_2$  and  $R_1=R_2$ . Our findings indicate that OP at  $U_1$  is consistently higher than that at  $U_2$ . Furthermore, the results demonstrate that when the value of  $a_2$  is lower ( $0.5 < a_2 < 0.83$ ), OP at  $U_2$  is higher than that at  $U_1$ . Conversely, when  $a_2$  is higher ( $0.83 < a_2 < 1$ ), OP at  $U_2$  is lower than that at  $U_1$ . Additionally, our analytical expressions reveal that both  $\theta$  and  $\rho$  significantly impact ECs. Specifically, we observe that as  $\theta$  increases, EC decreases. Similarly, as  $\rho$  increases, EC also increases. For future work, we propose the development of a system that employs multiple antennas at a BS, benefiting both users  $U_1$  and  $U_2$ , to enhance system performance.

## ACKNOWLEDGEMENT

Authors acknowledges the support of time and facilities from Industrial University of Ho Chi Minh City for this study.

## REFERENCES




- [1] H. Q. Tran, C. V. Phan and Q. -T. Vien, "A power-splitting relaying protocol for wireless energy harvesting and information processing in NOMA systems," *IET Communications*, vol. 13, no. 14, pp. 2132-2140, 2019, doi: 10.1049/iet-com.2018.5897.
- [2] H. Q. Tran, C. V. Phan, and Q. -T. Vien, "Power splitting versus time switching based cooperative relaying protocols for SWIPT in NOMA systems," *Physical Communication*, vol. 41, 2020, doi: 10.1016/j.phycom.2020.101098.
- [3] H. Q. Tran, C. V. Phan, and Q. -T. Vien, "Performance analysis of power-splitting relaying protocol in SWIPT based cooperative NOMA systems," *EURASIP Journal on Wireless Communications and Networking*, vol. 110, pp. 1-26, 2021, doi:10.1186/s13638-021-01981-9.
- [4] A. Alqahtani, E. Alsusa, and A. Al-Dweik, "On the Performance of Cooperative IoT Using NOMA With Indoor-Outdoor Device Deployment," in *IEEE Systems Journal*, vol. 18, no. 2, pp. 917-928, 2024, doi: 10.1109/JSYST.2024.3359236.
- [5] H. Q. Tran, "Two Energy Harvesting Protocols for SWIPT at UAVs in Cooperative Relaying Networks of IoT Systems," *Wireless Pers Commun*, vol. 122, pp. 3719-3740, 2022, doi: 10.1007/s11277-021-09108-5.
- [6] S. N. Sur, D. Kandari, Ad. Silva, N. D. Nguyen, S. Nandi, and D. T. Do, "Hybrid Precoding Algorithm for Millimeter-Wave Massive MIMO-NOMA Systems," *Electronics*, vol. 11, no. 14, p. 2198, 2022, doi: 10.3390/electronics11142198.
- [7] T. Le-Thanh and K. Ho-Van, "MIMO NOMA with Nonlinear Energy Harvesting and Imperfect Channel Information," *Arabian Journal for Science and Engineering*, vol. 49, pp. 6675-6693, 2024, doi: 10.1007/s13369-023-08401-8.
- [8] A. Apiyo and J. Izydorczyk, "A Survey of NOMA-Aided Cell-Free Massive MIMO Systems," *Electronics*, vol. 13, no. 1, p. 231, 2024, doi: 10.3390/electronics13010231.
- [9] X. X. Nguyen and D. T. Do, "Optimal power allocation and throughput performance of full-duplex DF relaying networks with wireless power transfer-aware channel," *J Wireless Com Network*, 152, 2017, doi: 10.1186/s13638-017-0936-x.
- [10] M. B. Shahab and S. Y. Shin, "Time Shared Half/Full-Duplex Cooperative NOMA With Clustered Cell Edge Users," in *IEEE Communications Letters*, vol. 22, no. 9, pp. 1794-1797, 2018, doi: 10.1109/LCOMM.2018.2853627.
- [11] Q. Li, R. Q. Hu, Y. Qian, and G. Wu, "Cooperative communications for wireless networks: techniques and applications in LTE-advanced systems," in *IEEE Wireless Communications*, vol. 19, no. 2, pp. 22-29, 2012, doi: 10.1109/MWC.2012.6189409.
- [12] T. -T. -H. Nguyen and X. -N. Tran, "Performance of Cooperative NOMA System with a Full-Duplex Relay over Nakagami-m Fading Channels," *2019 3rd International Conference on Recent Advances in Signal Processing, Telecommunications & Computing (SigTelCom)*, Hanoi, Vietnam, pp. 130-134, 2019, doi: 10.1109/SIGTELCOM.2019.8696186.






- [13] L. Song, R. Wichman, Y. Li, and Z. Han, "Full-Duplex MIMO Communications. In Full-Duplex Communications and Networks," Cambridge: Cambridge University Press, pp. 109-137, 2017, doi:10.1017/9781316662106.005.
- [14] M. F. Kader, S. Y. Shin, and V. C. M. Leung, "Full-Duplex Non-Orthogonal Multiple Access in Cooperative Relay Sharing for 5G Systems," in *IEEE Transactions on Vehicular Technology*, vol. 67, no. 7, pp. 5831-5840, 2018, doi: 10.1109/TVT.2018.2799939.
- [15] Q. Hussain, "On the Capacity Analysis Performance of ASIC Based Hybrid Full and Half Duplex User Relaying Cooperative NOMA System," *Wireless Personal Communications*, vol. 131, no. 4, pp. 2627-2647, 2023, doi: 10.1007/s11277-023-10561-7.
- [16] X. Xie, Y. Bi, "Fundamental Limits of Full-Duplex Spectrum Sharing Under Peak Interference Power Constraint," *Wireless Personal Communications*, vol. 124, pp. 1423-1441, 2022, doi: 10.1007/s11277-021-09412-0.
- [17] G. Li, H. Liu, and G. Huang, "Effective capacity analysis of reconfigurable intelligent surfaces aided NOMA network," *J Wireless Com Network*, vol. 198, 2021, doi: 10.1186/s13638-021-02070-7
- [18] X. Zhang, X. Yue, and S. Kang, "Effective Capacity Analysis of NOMA Networks with Short Packets," *Applied Sciences*, vol. 11, no. 23, p. 11438, 2021, doi: 10.3390/app112311438.
- [19] G. Huang *et al.*, "Effective capacity analysis of NOMA with transceiver hardware and SIC imperfections," *Physical Communication*, vol. 58, p. 102039, 2023, doi: 10.1016/j.phycom.2023.102039.
- [20] X. Li, H. Liu, G. Li, Y. Liu, M. Zeng, and Z. Ding, "Effective Capacity Analysis of AmBC-NOMA Communication Systems," in *IEEE Transactions on Vehicular Technology*, vol. 71, no. 10, pp. 11257-11261, Oct. 2022, doi: 10.1109/TVT.2022.3186871.
- [21] X. Yue, Y. Liu, S. Kang, A. Nallanathan, and Z. Ding, "Exploiting Full/Half-Duplex User Relaying in NOMA Systems," in *IEEE Transactions on Communications*, vol. 66, no. 2, pp. 560-575, 2018, doi: 10.1109/TCOMM.2017.2749400.
- [22] C.-B. Le and D.-T. Do, "Performance analysis of downlink NOMA relying energy harvesting and full-duplex," *ECTI Transactions on Computer and Information Technology (ECTI-CIT)*, vol. 16, no. 1, pp. 1-9, 2022, doi: 10.37936/ecti-cit.2022161.242809.
- [23] D. Wu and R. Negi, "Effective capacity: a wireless link model for support of quality of service," in *IEEE Transactions on Wireless Communications*, vol. 2, no. 4, pp. 630-643, 2003, doi: 10.1109/TWC.2003.814353.
- [24] E. Hildebrand, "Introduction to Numerical Analysis," *Dover: New York, NY, USA*, 1987, doi: 10.1007/978-0-387-21738-3.
- [25] I. S. Gradshteyn, and I. M. Ryzhik, "Table of integrals, series, and products," 7th ed. *San Diego, CA, USA: Academic*, 2007, doi: 10.1016/C2010-0-64839-5.
- [26] Y. Cheng, K. H. Li, Y. Liu, K. C. Teh, and H. V. Poor, "Downlink and Uplink Intelligent Reflecting Surface Aided Networks: NOMA and OMA," in *IEEE Transactions on Wireless Communications*, vol. 20, no. 6, pp. 3988-4000, Jun. 2021, doi: 10.1109/TWC.2021.3054841.

## BIOGRAPHIES OF AUTHORS



**Huu Q. Tran**    received the M.S degree in Electronics Engineering from Ho Chi Minh City University of Technology and Education (HCMUTE), Vietnam in 2010. Currently, he has been working as a lecturer at Faculty of Electronics Technology, Industrial University of Ho Chi Minh City (IUH), Vietnam. He obtained his doctorate from the Faculty of Electrical and Electronics Engineering at HCMUTE, Vietnam. His research interests include wireless communications, non-orthogonal multiple access (NOMA), energy harvesting (EH), wireless cooperative relaying networks, heterogeneous networks (HetNet), cloud radio access networks (C-RAN), unmanned aerial vehicles (UAV), reconfigurable intelligent surfaces (RIS), short-packet communication (SPC), and internet of things (IoT). He can be contacted at email: tranquyhuu@iuh.edu.vn.



**Samarendra Nath Sur**    received M.Sc. degree in Electronics Science from Jadavpur University in 2007 and M.Tech. degree in Digital Electronics and Advanced Communication from Sikkim Manipal University in 2012 and Ph.D. degree in MIMO signal processing from National Institute of Technology (NIT), Durgapur, in 2019. Since 2008, he has been associated with the Sikkim Manipal Institute of Technology, India, where he is currently an assistant professor (SG) in the Department of Electronics and Communication Engineering. His current research interests include broadband wireless communication (MIMO and spread spectrum technology), advanced digital signal processing, remote sensing, and radar image/signal processing (soft computing). He can be contacted at email: samarendra.s@smit.smu.edu.in.